TU/e EINDHOVEN UNIVERSITY OF TECHNOLOGY

Low-dose (S)TEM elemental analysis of water and oxygen uptake in beam sensitive materials

Citation for published version (APA):
Leijten, Z. J. W. A., Wirix, M. J. M., Strauss, M., Plitzko, J. M., de With, G., & Friedrich, H. (2020). Low-dose (S)TEM elemental analysis of water and oxygen uptake in beam sensitive materials. *Ultramicroscopy*, *208*, Article 112855. https://doi.org/10.1016/j.ultramic.2019.112855

Document license:
CC BY-NC-ND

DOI:
10.1016/j.ultramic.2019.112855

Document status and date:
Published: 01/01/2020

Document Version:
Publisher's PDF, also known as Version of Record (includes final page, issue and volume numbers)

Please check the document version of this publication:

• A submitted manuscript is the version of the article upon submission and before peer-review. There can be important differences between the submitted version and the official published version of record. People interested in the research are advised to contact the author for the final version of the publication, or visit the DOI to the publisher's website.
• The final author version and the galley proof are versions of the publication after peer review.
• The final published version features the final layout of the paper including the volume, issue and page numbers.

Link to publication

General rights
Copyright and moral rights for the publications made accessible in the public portal are retained by the authors and/or other copyright owners and it is a condition of accessing publications that users recognise and abide by the legal requirements associated with these rights.

• Users may download and print one copy of any publication from the public portal for the purpose of private study or research.
• You may not further distribute the material or use it for any profit-making activity or commercial gain
• You may freely distribute the URL identifying the publication in the public portal.

If the publication is distributed under the terms of Article 25fa of the Dutch Copyright Act, indicated by the "Taverne" license above, please follow below link for the End User Agreement:

www.tue.nl/taverne

Take down policy
If you believe that this document breaches copyright please contact us at:

openaccess@tue.nl

providing details and we will investigate your claim.

Download date: 16. Nov. 2023

Ultramicroscopy 208 (2020) 112855

Contents lists available at ScienceDirect

Ultramicroscopy

journal homepage: www.elsevier.com/locate/ultramic

Low-dose (S)TEM elemental analysis of water and oxygen uptake in beam sensitive materials

Z.J.W.A. Leijten[a,b,c], M.J.M. Wirix[d], M. Strauss[e,f], J.M. Plitzko[g], G. de With[a,b], H. Friedrich[a,b,c,*]

[a] Laboratory of Materials and Interface Chemistry, Department of Chemical Engineering and Chemistry, Eindhoven University of Technology, Het Kranenveld 14, Postbus 513, 5600 MB, Eindhoven, the Netherlands.
[b] Center for Multiscale Electron Microscopy, Eindhoven University of Technology, Het Kranenveld 14, Postbus 513, 5600 MB, Eindhoven, the Netherlands
[c] Institute for Complex Molecular Systems, Eindhoven University of Technology, De Zaale, 5612 AJ Eindhoven, the Netherlands
[d] Materials & Structural Analysis, Thermo Fisher Scientific, Achtseweg Noord 5, 5651 GG, Eindhoven, the Netherlands
[e] CryoEM Facility, Max Planck Institute of Biochemistry, Am Klopferspitz 18, Martinsried, Germany
[f] Department of Anatomy and Cell Biology, McGill University, Montreal, Canada
[g] Department of Molecular Structural Biology, Max Planck Institute of Biochemistry, Am Klopferspitz 18, Martinsried, Germany

ARTICLE INFO

Keywords:
Low-dose
cryo STEM-EELS
cryo EFTEM
Direct electron detector
Electron beam damage
Organic photovoltaics
Oxygen uptake
Water uptake

ABSTRACT

The performance stability of organic photovoltaics (OPVs) is largely determined by their nanoscale morphology and composition and is highly dependent on the interaction with oxygen and water from air. Low-dose cryo-(S)TEM techniques, in combination with OPV donor-acceptor model systems, can be used to assess oxygen- and water-uptake in the donor, acceptor and their interface. By determining a materials dependent critical electron dose from the decay of the oxygen K-edge intensity in Electron Energy Loss Spectra, we reliably measured oxygen- and water-uptake minimizing and correcting electron beam effects. With measurements below the dose limit the capability of STEM-EDX, EFTEM and STEM-EELS techniques are compared to qualitatively and quantitatively measure oxygen and water uptake in these OPV model systems. Here we demonstrate that oxygen and water is mainly taken up in acceptor-rich regions, and that specific oxygen uptake at the donor-acceptor interphase does not occur. STEM-EELS is shown to be the best suitable technique, enabling quantification of the local oxygen concentration in OPV model systems.

1. Introduction

The demand for renewable energy is increasing rapidly as more and more actions are taken to combat climate change. Organic photovoltaics (OPVs) are a possible means of providing this renewable energy, due to their ease of processing. However, organic photovoltaics degrade much more rapidly than silicon photovoltaics, especially in the presence of oxygen and water [1,2].

The performance of OPVs is highly dependent on their morphology and chemical composition. Generally, they are composed of domains of donor and acceptor materials [3]. Morphology changes due to degradation can cause phase domains to become larger than the exciton diffusion length, while chemical changes can shift energy levels or decrease the amount of light that can be absorbed [2,4]. Furthermore, the interface between donor and acceptor domains plays an important role, since power generation in OPVs takes place at this interface. (Chemical) changes at the interface are therefore expected to have a large effect on the overall performance of the OPV device, due to, e.g., changes in energy levels upon oxygen and water uptake [5,6]. Whether oxygen and water uptake occurs mainly in the donor or acceptor phase, or at the interface, is a question that still needs to be resolved. Energy Filtered Transmission Electron Microscopy (EFTEM), Scanning Transmission Electron Microscopy combined with Electron Energy Loss Spectroscopy (STEM-EELS) and STEM combined with Energy Dispersive X-ray Spectroscopy (STEM-EDX) are techniques with the potential to resolve this question, both qualitatively and quantitatively.

Recently, EFTEM has been applied to analyze both the morphology and the nanoscale composition of OPVs [7–9]. EFTEM has helped to gain understanding of, amongst others, the crystallization induced demixing of poly(3-hexylthiophene) (P3HT) and Phenyl-C_{61}-Butyric acid Methyl ester (PCBM), common OPV materials [7]. Furthermore, EFTEM has been used to visualize a mixed donor and acceptor phase between the separate P3HT and PCBM phases in a P3HT:PCBM bulk heterojunction, which indicates a separate interphase [8]. Additionally, STEM-EELS has been employed to analyze the effect of fullerene size on the OPV morphology [9], while STEM-EDX has been used to analyze

* Corresponding author at: Department of Chemical Engineering and Chemistry, Eindhoven University of Technology, 5612AJ Eindhoven, the Netherlands.
E-mail address: h.friedrich@tue.nl (H. Friedrich).

https://doi.org/10.1016/j.ultramic.2019.112855
Received 13 November 2018; Received in revised form 18 July 2019; Accepted 7 October 2019
Available online 10 October 2019
0304-3991/ © 2019 The Authors. Published by Elsevier B.V. This is an open access article under the CC BY-NC-ND license (http://creativecommons.org/licenses/BY-NC-ND/4.0/).

and localize interfaces in small-molecule photovoltaics [10].

A drawback of (S)TEM-based analysis is the comparatively high dose used to image the sample. OPV materials are electron beam sensitive, meaning that their properties will change during exposure to the electron beam [11–15]. Beam damage can be seen as, e.g., the decrease of diffraction ring intensity [12,13], shrinkage or expansion across the illuminated area [12], and loss of elemental information [14,15]. Furthermore, mass loss can occur [16]. It has been shown that the extent of this beam damage can be reduced by temperature [12], meaning that OPV materials exhibit less decrease of diffraction ring intensity at cryogenic conditions. Furthermore, the amount of shrinkage and/or expansion also changes when going from room temperature to cryogenic conditions. More interestingly, at cryogenic conditions, an oxygen- and water-free sample preparation further stabilizes OPV materials [12]. Additionally, cryogenic conditions could prevent the boiling off of volatile species in high vacuum [17], which creates the possibility of measuring the presence of physisorbed oxygen and water using EFTEM, STEM-EELS or STEM-EDX, in addition to chemical changes (chemisorbed, i.e., chemically bonded water and oxygen) as a result of OPV degradation. In principle, STEM-EELS and STEM-EDX are more suited to low electron dose analysis, because of their ability to detect multiple elements in one acquisition, and simultaneous acquisition of the background. In EFTEM, three acquisitions are needed just for one element, significantly increasing the accumulated electron dose. However, EFTEM holds the advantage of acquiring a larger field of view, beneficial for statistical analysis, in relatively short acquisition times as compared to STEM-EELS and STEM-EDX [18].

The high electron doses required for EFTEM, STEM-EELS and STEM-EDX are thus likely to cause electron beam damage, making it difficult to acquire 3D elemental information using tomography [19], which would be necessary to resolve local chemical changes in a bulk heterojunction morphology, a bicontinuous network of donor and acceptor domains. Therefore, to visualize interface regions, model systems are necessary, making it possible to localize the interface region in 2D images [20,21]. Columnar model systems, with columns perpendicular to the sample plane, are best suited for this kind of analysis. To realize a corresponding columnar model system, sample preparation methods such as nanoimprint lithography [22,23] and block-copolymer self-assembly [24,25] can be utilized.

In this paper, columnar model systems are fabricated using the phase separation between P3HT and polystyrene [26,27]. After replacing the polystyrene with PCBM, this model system allows us to localize the interface region, and perform chemical analysis of the P3HT, PCBM and interphase regions from 2D micrographs. Cryogenic STEM-EELS, STEM-EDX and EFTEM will be used to measure the oxygen and water uptake in these P3HT:PCBM model systems, where a distinction will be made between the P3HT region, the PCBM region, and the interphase region. Electron beam damage is analyzed to guide experiments to maximize information content in the acquired data. Finally, a comparison between the three techniques is given, highlighting the benefits and drawbacks of each technique for the low-dose elemental analysis of OPV, and beam sensitive materials, in general.

2. Materials and methods

2.1. Materials

Chlorobenzene, polystyrene (PS, average M_w 35000 g/mol) and poly(3-hexylthiophene) (P3HT, Plexcore OS 2100) were acquired from Sigma Aldrich. The solvents acetone, dichloromethane (DCM, stabilized with Amylene) and 2-propanol were obtained from Biosolve. Solenne B.V. provided Phenyl-C_{61}-Butyric acid methyl ester (PCBM, 99.5% purity). TEM grids (carbon film on 200 mesh copper grids, CF200-Cu) were purchased from EMS Diasum. All materials were used as purchased.

2.2. Preparation of columnar OPV model system

22.5 mg P3HT and 7.5 mg PS were dissolved in 1 ml chlorobenzene. The solution was stirred at 70 °C for 24 h to completely dissolve the materials [26,27].

A custom-made specimen holder [12] was cleaned by ultrasonication in acetone for 30 min, followed by rubbing with soap and rinsing with demineralized water. Afterwards, the specimen holder was ultrasonicated in isopropanol for 30 min, followed by a final UV-ozone treatment for 30 min.

The P3HT-PS solution was spin-coated (using a Laurel WS-650-23NPP-LITE Spin Coater outside the glovebox and an SPS POLOS Spin 150i inside the glovebox) on a TEM grid loaded specimen holder at 2000 rpm for 1 min. The spin-coated TEM grid was removed from the specimen holder and submerged in acetone for 1 h to completely remove all PS, whilst stirring. Hereafter, the TEM grid was washed with acetone to achieve complete polystyrene removal. Afterwards, the washed TEM grid was loaded on a freshly cleaned specimen holder, and PCBM was spin-coated on top at 3000 rpm for 1 min. Samples were prepared in either a glovebox with inert atmosphere, or in air. Glovebox samples were submerged in liquid nitrogen, directly after leaving the glovebox (M-Braun Labmaster Glove Box System) to minimize exposure to air. Samples prepared in air were exposed to 100% humidity in a Vitrobot for 10 min before plunge-freezing in liquid ethane.

The model system was analyzed using large-area stitching, using the TU/e Acquisition Toolbox [28], on a Tecnai G2 Sphera microscope (Thermo Fisher Scientific, equipped with a LaB_6 and operated at 200 kV. Sulfur and thickness maps to assess the sample morphology (Fig. 2b and c) were acquired on the TU/E Cryo Titan (Thermo Fisher Scientific), operated at 300 kV, equipped with a field emission gun, a Gatan GIF 2002 and a 2k × 2k Gatan CCD camera.

2.3. Critical dose determination

EELS data was acquired on the TU/e Cryo Titan, as described above. The microscope was operated at cryogenic conditions. The spectra were acquired at an energy loss of 500 eV, with a dispersion of 0.5 eV/pixel, a dose rate of 5 e/Å^{2}s, an acquisition time of 1 s, and by summing 10 frames per spectrum.

To determine the oxygen K-edge intensity in the EEL spectra, a power law was fitted to the spectrum between 465 eV and 525 eV via a non-linear least squares method in MATLAB (Eq. (1), where I is the intensity (counts), x the energy loss (eV) and a and b are fitting parameters). This power law was extrapolated and subtracted from the spectrum between 535 and 565 eV, as background correction.

$$I = ax^{-b} \tag{1}$$

The total intensity of the background corrected signal between 535 and 565 eV, i.e., the oxygen peak, was plotted as a function of the accumulated electron dose. The loss in intensity of the oxygen peak in the EEL spectra was used as a criterion to quantify the beam-sensitivity of the sample and to determine the critical dose for all subsequent experiments. In EFTEM, the critical dose was only spent on the oxygen edge. Therefore, additional beam damage due to acquisition of pre-edge images, the sulfur map and the thickness map needed to be assessed using the normalized cross correlation coefficient method [12].

During combined STEM-EELS/EDX acquisition sub-pixel scanning was not active due to software restrictions. However, since sub-pixel scanning reduces the amount of radiation damage, the measured oxygen content without sub-pixel scanning is lower than with sub-pixel scanning, so that conclusions regarding the oxygen content remain valid.

2.4. Elemental mapping

Table 1 shows the total dose used, and pixel size and image size

Table 1
Electron doses, pixel sizes and image sizes of images acquired with EFTEM, STEM-EELS or STEM-EDX.

	EFTEM			STEM-EELS		STEM-EDX
	Oxygen	Sulfur	Thickness	Core Loss	Zero Loss	Spectrum
Total dose (e/Å^2)	1215	300	20	405	10	405
Pixel size (nm)	17.6			17.12		17.12
Image size	479 × 463 (after binning 8)			128 × 128		128 × 128

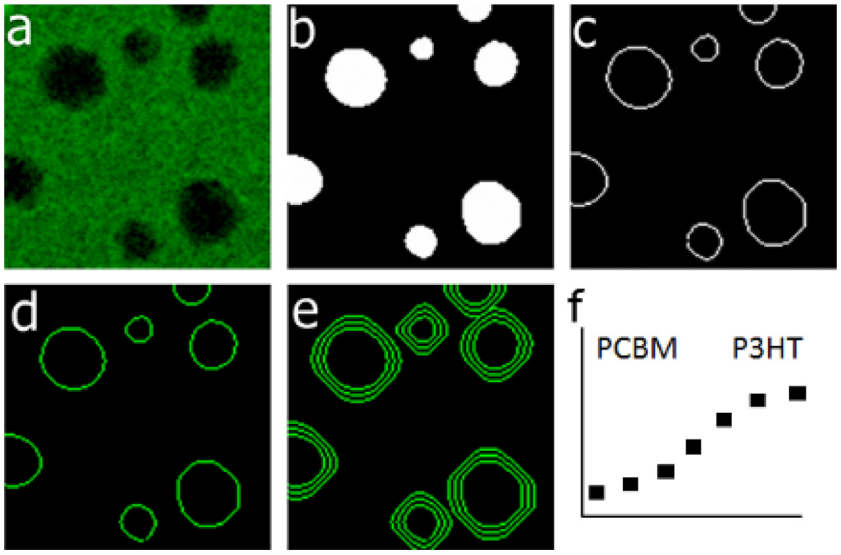

Fig. 1. (a) Sulfur map of a P3HT:PCBM model system, where the dark areas represent PCBM and the green areas represent P3HT. (b) Binary image of a. (c) Interface mask prepared from b. (d) Interface mask from c multiplied with the sulfur map of a. (e) Multiple interface mask multiplied with the sulfur map of a. (f) Interface intensity profile calculated by taking the average pixel intensity of each set of rings from e, where the internal ring is the data point on the left of the graph. The size of the sulfur map is 1.994 μm × 1.994 μm. (For interpretation of the references to color in this figure legend, the reader is referred to the web version of this article.)

acquired with each technique. The calculated critical dose was used to acquire the oxygen K-edge signal, and the pixel size was kept at a similar size between techniques. Due to the lack of beam-sensitivity of the sulfur and thickness signal (see Supporting Information, Section 4), the conditions for the sulfur and thickness map were selected based on the amount of contrast between the two phases.

STEM-EELS and STEM-EDX maps of the columnar model system were acquired simultaneously on a Talos F200X (Thermo Fisher Scientific) at Nanoport Eindhoven, operated at 200 kV under cryogenic conditions, equipped with a field emission gun with X-FEG emitter. The EELS signal was acquired with a Gatan Enfinium Spectrometer and a Ceta 16M CMOS camera. The EDX signal was acquired using a Thermo Scientific 4SDD ED/SuperX system. A Gatan cryo holder was used. The magnification was set to 57 kx, using a camera length of 60 mm. The convergence semi-angle was 10 mrad, while the collection semi-angle was 30 mrad.

EFTEM was performed on the Thermo Fisher Scientific Titan Krios, located in the Max Planck Institute for Biochemistry, Martinsried, Germany. The microscope was operated at 300 kV under cryogenic conditions, equipped with a field-emission gun, a Gatan Quantum GIF, an autoloader and a Gatan K2 direct electron detector. The magnification was set at 6.5 kx at a dose rate of 3.5 e/Å^2.

In STEM-EELS, a core loss spectrum, including the sulfur L edge and the oxygen K edge, was acquired at a dose of 405 e/Å^2. A STEM-EDX spectrum was acquired simultaneously. In EFTEM, the oxygen K edge was acquired at a dose of 405 e/Å^2 using a slit width of 30 eV, positioned around 547 eV. Both pre-edge images (where the slit was positioned around 514 eV and 484 eV), at a dose of 405 e/Å^2 per image. Furthermore, in EFTEM, a sulfur map needs to be acquired separately. To balance beam effects and signal to noise ratio, a total dose of 100 e/Å^2 was chosen to acquire the sulfur L edge, using a slit width of 20 eV, centered on 180 eV. The post-edge images were acquired at the same dose per image, where the slit was centered on 514 and 484 eV.

A zero-loss spectrum was acquired in STEM-EELS using a dose of 10 e/Å^2. In EFTEM, a zero-loss filtered image and an unfiltered image were acquired using a dose of 10 e/Å^2 per image, where a slit width of 20 eV was used for the zero-loss filtered image.

In STEM-EELS and STEM-EDX, spectrum images were acquired with 128 × 128 × 2048 pixels with a pixel size of 17.12 nm. Oxygen and sulfur maps were extracted in Digital Micrograph, were plural scattering was removed using Fourier-ratio deconvolution. In EFTEM, images were acquired with 3838 × 3710 pixels with a pixel size of 2.2 nm. After acquisition, the images were binned with a factor of 8, which led to images with 479 × 463 pixels with a pixel size of 17.6 nm. Dose fractionation was employed, where the post-edge, pre-edge 2 and pre-edge 1 image were each made up of 120 images with an exposure time of 1 s. These images were summed to create the final post-edge and pre-edge images.

In principle, a larger area could have been acquired in EFTEM, with a pixel size of 17.6 nm before binning. However, this would lead to the illuminated area being smaller than the image, showing that the magnification could not be lowered further.

The thickness maps were used to quantify the thickness of the sample. Supporting Information section 1 shows the formula, and its deduction, that is used to quantify the thickness from the thickness maps.

2.5. Data analysis by smart averaging

To find the oxygen intensity of each phase, a binary image is created from the sulfur map using Otsu thresholding [29]. The average intensity and the standard deviation of the PCBM and P3HT region is subsequently calculated in Matlab, by multiplying either the P3HT or PCBM binary image with the oxygen map.

To assess oxygen and water uptake in either the P3HT, PCBM or interphase, interface plots are created by smart averaging, as shown in Fig. 1. The data analysis was performed in Matlab, using Otsu thresholding [29] to convert a sulfur map (Fig. 1a) into a binary image (Fig. 1b). This binary image was converted into an interface mask (Fig. 1c), by first shrinking the object (using the bwmorph ('shrink')

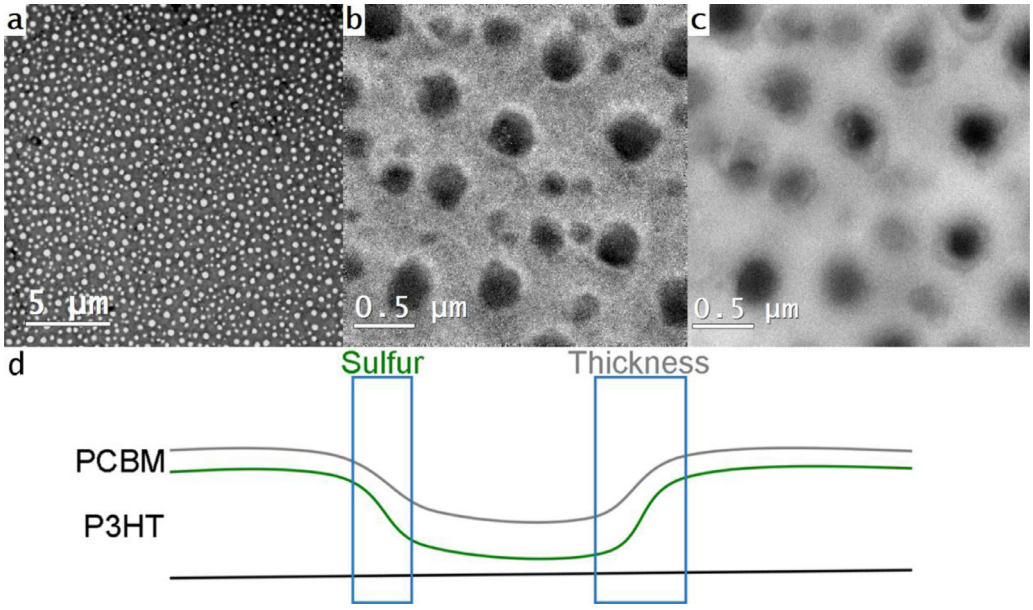

Fig. 2. (a) Large area image of the P3HT:PCBM model system, where PCBM is shown as the light circles, due to a lower thickness. (b) Sulfur map of the P3HT:PCBM model system. (c) Thickness map of the P3HT:PCBM model system. (d) Schematic cross section of an average PCBM feature in the P3HT:PCBM model system.

command in Matlab), and subtracting this image from the original binary image. The interface mask was multiplied with the original sulfur map (or oxygen or thickness map, Fig. 1d), where the average intensity of the interior of the rings was calculated. By repeating the shrinking or thickening (bwmorph, 'thicken) of the interface mask (Fig. 1e), and subsequently calculating the average intensity of each set of rings, an interface profile was created (Fig. 1f).

3. Results and discussion

3.1. Columnar model system

Fig. 2a shows the P3HT:PCBM model system, where the light areas represent PCBM and the dark areas represent P3HT. The PCBM regions in this case are lighter due to a lower thickness of the PCBM regions as compared to the P3HT regions. For equal P3HT and PCBM thickness, PCBM would be the darker phase in bright field TEM in underfocus. [30,31] An oxygen and sulfur map, acquired using EFTEM, are shown in Fig. 2b and c. Using the smart averaging scheme, as explained in Section 2.5, we investigated the average shape of the PCBM structures (details are shown in the Supporting Information, Section 2). A schematic of the cross-sectional sample morphology is shown in Fig. 2d, showing a relatively narrow P3HT transition and a broader total thickness transition. The schematic indicates that the interface is not completely perpendicular to the sample. Therefore, to completely separate the P3HT-rich, PCBM-rich and interface rich region, not only oxygen maps are required, but sulfur maps are required to localize P3HT and estimate the P3HT thickness, and thickness maps are necessary to find the total thickness. Combining this information, the separate P3HT and PCBM thickness can be calculated, and, hence, the oxygen content of each phase. This model system is further used to measure oxygen and water uptake, using cryogenic STEM-EELS, EFTEM and STEM-EDX.

3.2. Critical dose calculation

A critical dose, i.e., the maximum electron dose that can be used before the acquired information becomes unreliable, is calculated by following the intensity of the oxygen K-edge as a function of accumulated dose, as shown in Fig. 3. In Fig. 3a one can see an EEL spectrum of a fresh sample and a sample that has been exposed to 1000 e/Å^2, where a clear decrease in intensity is visible. We hypothesize that the remaining oxygen K edge originates from the oxygen atoms that are present in the PCBM molecular structure, as the shape of the edge is similar to the shape of the oxygen K edge of a PCBM sample (see Supporting Information Section 3).

In general, the SNR (Eq. 2, where *SNR* is the signal-to-noise ratio, I_k is the K edge intensity (counts), I_b is the background intensity (counts) and h is a parameter dependent on the quality of the background fit [32,33]), increases as a function of accumulated dose, since the relative contribution of shot-noise (defined as the square root of the total intensity). However, this is not true for beam-sensitive materials, since the intensity of, in this case, the oxygen K edge decreases as a function of accumulated dose (as shown in Fig. 3), following Eq. 3, where I_k is the oxygen K-edge intensity (counts), D is the accumulated electron dose (e/Å^2), α and β are fitting parameters, and I_∞ is the oxygen K-edge intensity at an infinite electron dose (counts).

$$SNR = \frac{I_k}{\sqrt{I_k + h\ I_b}} \tag{2}$$

$$\frac{\partial I_k}{\partial D} = \alpha e^{\frac{-D}{\beta}} (+\ I_\infty) \tag{3}$$

By combining equation the derivative of Eq. (2), and Eq. (3), we can now calculate the SNR of the added signal ($\partial SNR/\partial D$) as shown in Eq. (4). Since the intensity of the background is not dependent on the electron dose (see Supporting Information, Section 4), we can write $\partial I_b/\partial D$ as b, the background intensity (counts). We define the critical dose as the dose where $\partial SNR/\partial D$ is 5, a modified take on the Rose criterion. At the dose at which $\partial SNR/\partial D$ is lower than 5, the information that is added to the image or spectrum is unreliable, and will only lower the SNR. By fitting Eq. (3) to the data shown in Fig. 3b, and filling in the obtained fitting parameters in Eq. (4), we obtain a critical dose of 405 e/Å^2. For the factor h, a conservative literature value of 4.5 is used [34]. The entire calculation and the values of the parameters are shown in the Supporting Information, Section 5.

$$\frac{\partial SNR}{\partial D} = \frac{\frac{\partial I_k}{\partial D}}{\sqrt{\frac{\partial I_k}{\partial D} + h \times \frac{\partial I_b}{\partial D}}} = \frac{\alpha e^{\frac{-D}{\beta}}}{\sqrt{\alpha e^{\frac{-D}{\beta}} + hb}} \tag{4}$$

Most importantly, Eq. (3) can further be used to correct the

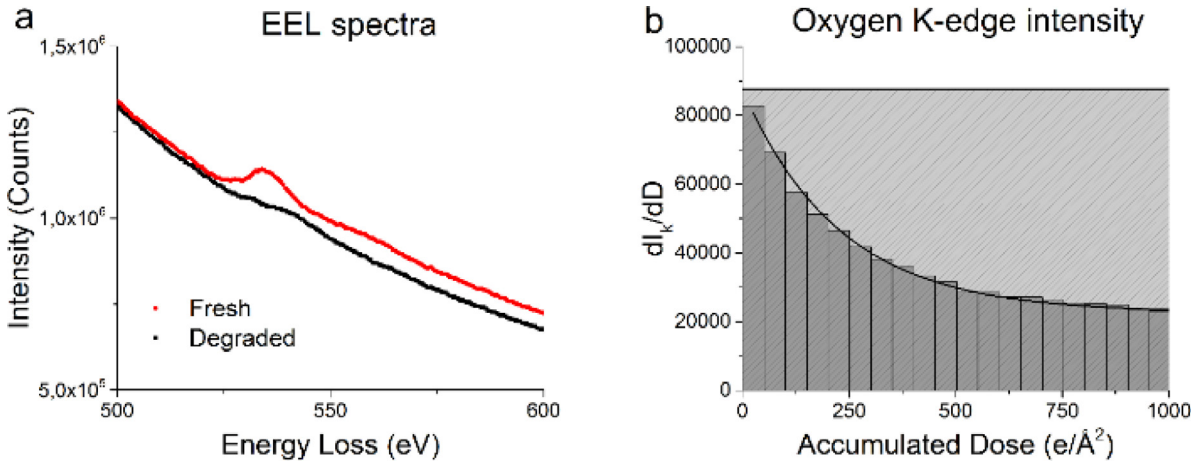

Fig. 3. (a) shows the oxygen K-edge of a sample that is exposed to 50 e/Å^2 (red, fresh) and a sample that has been subjected to 1000 e/Å^2 (black, degraded). Fig. b shows the oxygen K-edge intensity as a function of accumulated dose. A fit with an exponential decay is shown, following the decay of the oxygen K-edge intensity. The total area under the exponential decay curve is the total oxygen intensity that will be measured at a certain accumulated dose. The light gray square indicates the intensity that would have been measured if the sample would have been beam-stable. The ratio between the two areas can be used to correct for electron beam effects and to approximate the original oxygen concentration. (For interpretation of the references to color in this figure legend, the reader is referred to the web version of this article.)

measured oxygen signal and assess the initial composition as shown by the rectangle in Fig. 3b. We assume that this works independent of dose rate and imaging conditions. This is due to the fact that the ratio between the integral of Eq. (3) (from 0 to 405 e/Å^2) and the extrapolated initial EELS spectrum, i.e., the oxygen intensity without the effects of beam damage, can be approximated (Fig. 3b), leading to a correction factor of 1.65 at an accumulated dose of 405 e/Å^2 (see Supporting Information, Section 6 for more details). By multiplying the measured oxygen content with this correction factor we compensate for the oxygen that is lost during acquisition and are able to estimate the initial oxygen concentration.

The beam stability of the sulfur and thickness maps was assessed according to literature [12], as is shown in Supporting Information, Section 7.

In conclusion, the critical dose to acquire a reliable oxygen map is defined as the electron dose where the added signal has an SNR smaller than 5, and this critical dose is calculated to be 405 e/Å^2, based on the decay of the oxygen K edge intensity. Furthermore, the final intensity of the oxygen K edge intensity can be multiplied by a factor of 1.65 to find the actual oxygen content.

3.3. Elemental imaging

Fig. 4 shows oxygen (a–c) and sulfur maps (e–g) of the P3HT:PCBM model systems, exposed to oxygen and water, acquired using either STEM-EDX, EFTEM, and STEM-EELS using the calculated critical electron dose of 405 e/Å^2, showing the oxygen K edge intensity (counts). By using the sulfur maps to localize the P3HT-rich (high sulfur intensity) and PCBM-rich (low sulfur intensity) regions it is clearly visible that the oxygen maps acquired using STEM-EELS show the most contrast between the P3HT-rich and PCBM-rich regions. Table 2 shows the average intensities and their standard deviation. The intensity of the oxygen K edge is higher in the PCBM-rich regions, independent of the technique that is used. Although the difference in intensity is small when using STEM-EDX or EFTEM, the difference in intensity is statistically significant (see Supporting Information, Section 8).

In terms of SNR, as defined by the ratio of the average intensity and the standard deviation of the average intensity, we see that EFTEM gives the lowest SNR, followed by STEM-EDX and STEM-EELS. This is likely to be caused by the poor quality of the calculated background (i.e., a higher h factor in Eq. (2)) that is inherent in EFTEM. In STEM-EDX, the low SNR is caused by the small amount of X-rays hitting the detector. Due to the lack of background in STEM-EDX the critical dose calculated in Eq. (4) is not valid. However, for a fair comparison, and to simultaneously acquire STEM-EDX and STEM-EELS data, the dose is kept the same. The lack of background signal in STEM-EDX ensures that the standard deviation of the intensity, i.e., the noise level, is approximately the square root of the average intensity, showing that mainly shot-noise contributes to the noise in STEM-EDX.

STEM-EELS gives a higher SNR than EFTEM [35], most likely due to the improved quality of the background fit, and a higher SNR than STEM-EDX, most likely due to the higher intensity at the detector and therefore a relatively lower contribution of shot-noise. Furthermore, the STEM-EELS results are the only results where the SNR is larger than the Rose criterion, indicating that reliable data is obtained. In principle, the SNR that is calculated can be compared to the SNR that is expected at the critical dose, using the integral of Eq. (4). When these numbers do not coincide, it is likely that the h-factor from literature is incorrect, and a better approximation of the h-factor could have been made.

The data analysis protocol, where a hyperbolic tangent equation is fitted to a calculated interface profile, as described in the materials and methods section, has been performed on each oxygen map (see Supporting information, Section 9), and has led to an R^2 value for each interface profile, as shown in Table 2. It is clearly visible that the STEM-EDX results show the lowest significance when calculating this interface profile. Due to the large area that is acquired in the EFTEM image, the R^2 value is much larger for the EFTEM results. In principle, larger areas can also be acquired using STEM-EDX (and STEM-EELS), which however significantly increases the total acquisition time.[18] STEM-EELS results do not only exhibit the highest SNR, but also show the largest R^2 when calculating an interface profile. This leads to the conclusion that 1) all three techniques can be used to assess a difference in oxygen intensity between phases, and 2) EFTEM and STEM-EELS can be used to reliably assess trends across P3HT:PCBM interfaces, using the data analysis protocol described in the materials and methods section. Due to the high SNR of the STEM-EELS results, the only technique leading to an SNR larger than 5, these results will further be used to quantify the oxygen content.

Fig. 4c and d show STEM-EELS oxygen maps of a sample that is exposed to oxygen and water (c) and a sample that is prepared in an oxygen and water-free environment (d). A clear difference in intensity is visible, showing that the oxygen content is much higher for an exposed sample than for a sample prepared in an oxygen- and water-free environment, proving that the measured oxygen content of an exposed

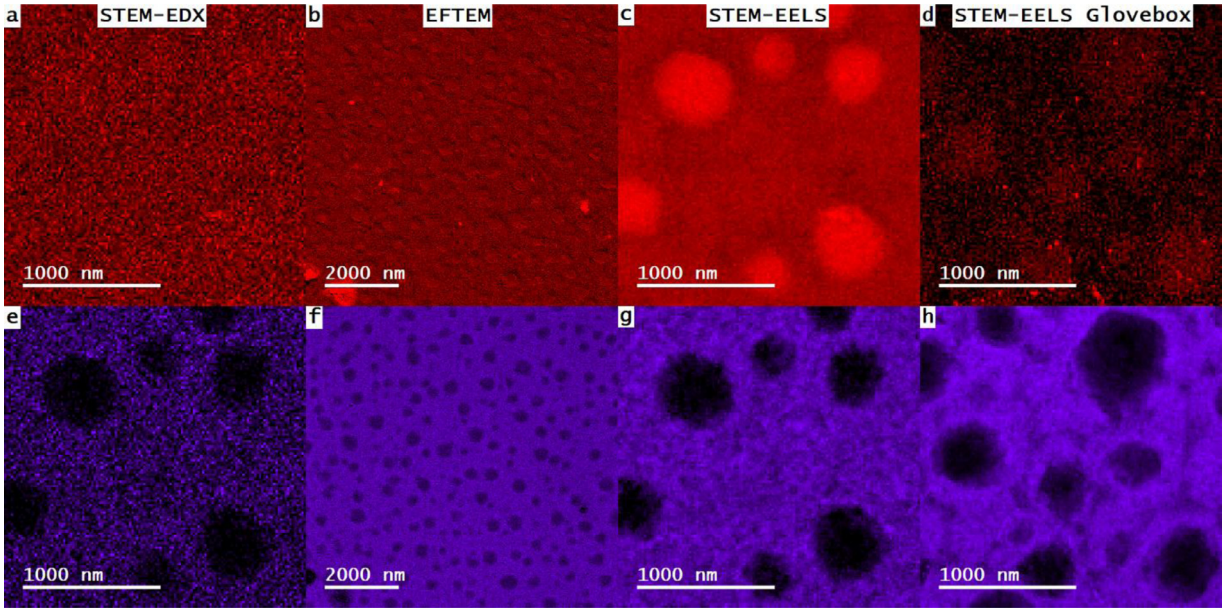

Fig. 4. (a–c)Oxygen maps of samples that are exposed to oxygen and water, acquired with STEM-EDX, EFTEM and STEM-EELS respectively. (d) Oxygen map of a sample prepared in an oxygen- and water-free glovebox, acquired with STEM-EELS. (e–g) Sulfur maps of samples shown in (a–c), acquired with STEM-EDX, EFTEM and STEM-EELS, respectively. (h) Sulfur map of the sample shown in (d). All the maps are shown in counts.

sample is indeed oxygen and water absorbed from the environment. Table 2 shows that, for the glovebox sample, the PCBM-rich region has the highest oxygen content, which is expected due to the oxygen atoms present in the PCBM molecular structure. The SNR of the glovebox sample is much lower, due to the lower intensity of the oxygen signal and therefore a larger contribution of shot-noise. To quantify both the oxygen and sulfur content, zero loss filtered images and thickness maps are necessary. The sulfur maps of both the exposed and glovebox sample are shown in Fig. 4g and h, while the thickness maps are shown in Fig. 5. It is clearly visible that the PCBM-rich islands are much thinner than the P3HT-rich matrix, as is confirmed by the average t/λ values of both regions (0.57 and 0.88 for the PCBM-rich and the P3HT-rich region of the exposed sample, respectively). By using the quantified sulfur map to calculate the P3HT-thickness, and by calculating the total thickness from the thickness map, the PCBM-thickness can be calculated (see Supporting Information, Section 10). Furthermore, this thickness can be used to calculate the oxygen content that is present in the molecular structure of PCBM using the size of the PCBM molecule (see Supporting Information, Section 10). This allows for a calculation of the total amount of oxygen and water that is physisorbed in each phase.

These calculations lead to the interface profiles in Fig. 6, based on the raw data provided in Supporting Information, Section 9. The initial oxygen concentration is multiplied with a factor of 1.65 to compensate for the intensity loss due to beam damage. In the PCBM-rich phase. 148 atoms/nm^2 are absorbed in a 62 nm film, leading to an oxygen concentration of 2.4 atoms/nm^3. In the P3HT-rich regions, 73 atoms/nm^2 are absorbed in a 138 nm film, leading to an oxygen concentration of 0.5 atoms/nm^3 (see Table 3 and Supporting Information, Section 11 for more details). This confirms that the uptake of oxygen and water mainly occurs in the PCBM-rich region (see also Supporting Information, Section 12), as the concentration is ~5 times larger than in the P3HT-rich region. Furthermore, it is clear that there is no specific interface uptake.

The oxygen content in the glovebox sample is calculated to be 0.53 atoms/nm^3 in the PCBM-rich region (see Supporting Information, Section 12), which is far lower than what is expected based on the oxygen content of the PCBM molecule (1.74 atoms/nm^2). Some deviations could be caused by inherent errors in the STEM-EELS quantification process, such as deviations in inelastic cross-section (5–10% for K-edges and 10–20% for L-edges), uncertainty in the background model, since a power-law is assumed, and uncertainty in experimental parameters such as the collection and convergenge angle [33]. This, however, cannot explain the factor three deviation from the expected value (1.74 atoms/nm^3). Furthermore, the SNR is lower than 5, indicating that the data might be too noisy for proper quantitative analysis.

For a fair comparison between the glovebox and the exposed sample one must take into account the thickness difference between the two samples, as the exposed sample is much thicker. This leads to multiple scattering, which potentially lowers the measured concentration, despite the fact that plural scattering is removed in Digital Micrograph. If the measured concentration is indeed lower due to multiple scattering, the difference in oxygen concentration between the exposed and glovebox sample would be even larger.

Water deposition cannot be fully excluded, but no characteristic

Table 2
Average oxygen intensity, standard deviation of the oxygen intensity and the SNR in the PCBM-rich and P3HT-rich regions acquired with STEM-EDX, EFTEM and STEM-EELS. For STEM-EELS, a sample that is exposed to water and oxygen is shown, and a sample prepared in an oxygen- and water-free environment. Furthermore, the R^2 of the fitted hyperbolic tangent on the interface profile is shown.

	Oxygen intensity PCBM phase in counts (*SNR*)	Oxygen intensity P3HT phase in counts (*SNR*)	R^2 of tanh fit
STEM-EDX Exposed	12.3 ± 3.6 (*3.5*)	11.6 ± 3.4 (*3.4*)	0.527
EFTEM Exposed	302 ± 259 (1.2)	218 ± 227 (1.0)	0.988
STEM-EELS Exposed	16.4×10^3 ± 1.2 × 10^3 (*13.2*)	11.7 × 10^3 ± 1.2 × 10^3 (*9.2*)	0.999
STEM-EELS Glovebox	1.5×10^3 ± 0.7 × 10^3 (*1.9*)	1.0 × 10^3 ± 0.7 × 10^3 (*1.5*)	0.984

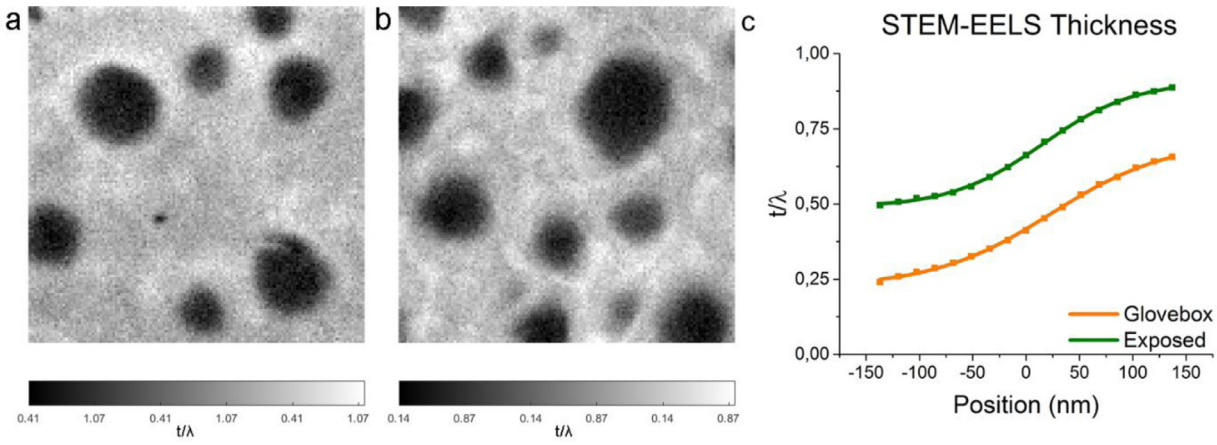

Fig. 5. (a) Thickness map of a sample exposed to oxygen and water, acquired with STEM-EELS. (b) Thickness map of a sample prepared in an oxygen- and water-free environment, acquired with STEM-EELS. (c). Thickness profile of a and b.

structures, such as leopard skin [36] have been observed. Furthermore, such residual water desorbs at electron doses much lower than the ones used here, so we believe that a possible influence of the microscope vacuum and/or residual adsorbed water on the sample surface on the experimental results can be neglected. As chemical bonding of water with the polymer does not change the water content and hardly any water is deposited, we surmise that beam-induced oxidation effects are not likely.

Furthermore, from the STEM-EELS thickness maps and intensity profiles (Fig. 5) it is clearly visible that not only the thickness, but also the shape of the PCBM islands differs between the two samples. Firstly, the total PCBM area seems to be larger in the glovebox sample, which is likely to be caused by differences in environmental conditions. Since P3HT is highly static in a glovebox, some P3HT might be removed from the sample vial after weighing, leading to a somewhat higher polystyrene content, causing larger polystyrene islands, and thus larger PCBM islands after spin-coating. Furthermore, the lack of oxygen and water might have an influence on the flow behavior during spin-coating, causing, e.g., different viscosities and different evaporation rates. Experimentally, it seems that the sample changes color faster, i.e., dries faster, during spin-coating in a lab environment than in a glovebox.

In summary, STEM-EELS is thus capable of measuring and quantifying a difference in oxygen and water uptake between the P3HT and PCBM regions, with a SNR higher than the Rose criterion. STEM-EELS shows that there is a ~5 times higher oxygen and water uptake in the PCBM-rich regions, and no specific uptake in the interphase is observed. By using thickness calculations based on sulfur and thickness maps, a distinction can be made between oxygen that is present in the molecular structure of PCBM, and oxygen and water that is absorbed from the environment.

4. Conclusions and outlook

We have compared low-dose cryogenic STEM-EDX, EFTEM and STEM-EELS to investigate the uptake of oxygen and water in a beam sensitive P3HT:PCBM model systems. By quantifying electron beam effects and determining the critical electron dose for the oxygen K edge signal, based on a desired signal-to-noise ratio, we have optimized data acquisition for our beam-sensitive model system. With this approach we are able to correct for the loss of oxygen signal due to electron beam damage.

All three techniques can be used to differentiate between samples exposed to water and oxygen and samples that are oxygen- and water-free. STEM-EDX and EFTEM give results with a signal-to-noise ratio below 5, but both techniques can still be used to calculate an intensity profile across the P3HT:PCBM transition, using a newly introduced smart averaging method. The EFTEM results show much larger significance than STEM EDX and can therefore be used to qualitatively assess trends in uptake.

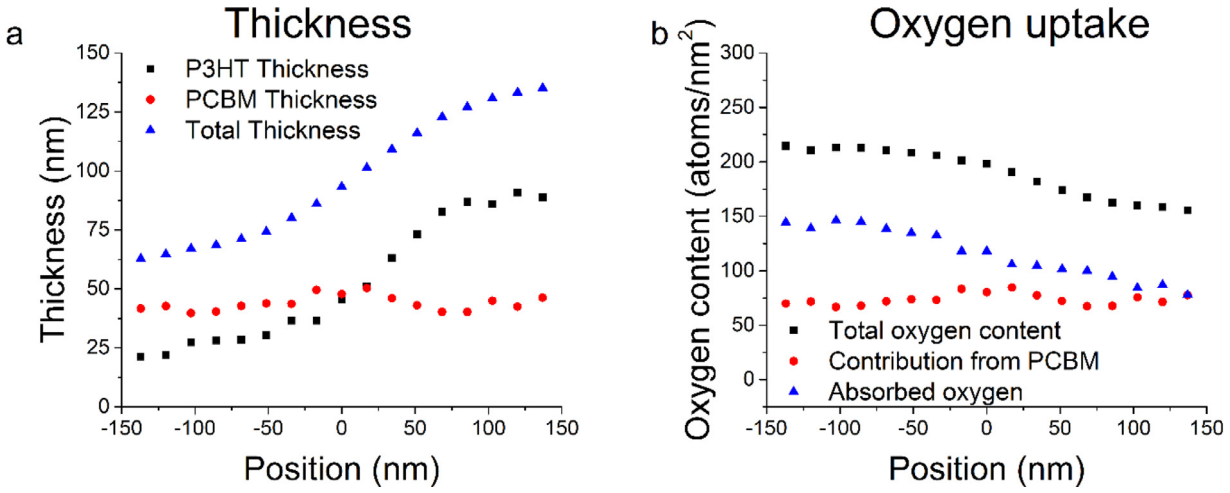

Fig. 6. (a) Thickness profiles of the P3HT layer, the PCBM layer and the combination of both layers from a P3HT:PCBM model system. (b) Oxygen content profiles of the total oxygen content, the oxygen content present in the PCBM molecular structure and the oxygen content absorbed from the environment.

Table 3
The total thickness, P3HT thickness, total oxygen content and the absorbed oxygen content of the P3HT-rich and PCBM-rich regions.

	Total thickness (nm)	P3HT thickness (nm)	Total oxygen content (atoms/nm^2)	Oxygen absorbed (atoms/nm^2)	Oxygen absorbed (atoms/nm^3)
P3HT-rich region	138	83	154	73	0.5
PCBM-rich region	62	23	213	148	2.4

STEM-EELS gives a signal-to-noise ratio that is higher than the Rose criterion of 5, and the acquired data can therefore be used to reliably quantify the oxygen and water concentration in the P3HT-rich and PCBM-rich regions. We measure for samples exposed to a humid and oxygen containing environment an uptake of 2.4 oxygen atoms/nm^3 in the PCBM-rich region, and an average uptake of 0.5 oxygen atoms/nm^3 in the P3HT-rich region. These values have been corrected for signal loss due to electron beam damage and oxygen atoms present in the PCBM molecular structure. Based on the calculated oxygen profiles across the P3HT-PCBM interphase we do not measure a specific interphase uptake.

The ability to measure and quantify oxygen and water uptake using STEM-EELS opens up possibilities in measuring OPV degradation due to the presence of oxygen and water. By changing the environment during sample preparation, we will be able to distinguish between chemisorbed and physisorbed oxygen and water in future, and thus distinguish between reversible and irreversible degradation in OPV model systems. Furthermore, the analysis techniques presented in this paper can be extended to other beam sensitive materials, especially materials whose functional properties are dependent on the presence of oxygen and water or other absorbed species.

Acknowledgments

We acknowledge financial support for this research from ADEM, A green Deal in Energy Materials of the Ministry of Economic Affairs of The Netherlands (www.adem-innovationlab.nl).

Supplementary materials

Supplementary material associated with this article can be found, in the online version, at doi:10.1016/j.ultramic.2019.112855.

References

[1] P. Cheng, X.W. Zhan, Stability of organic solar cells: challenges and strategies, chem. Soc. Rev. 45 (2016) 2544–2582.
[2] W.R. Mateker, M.D. mcgehee, Progress in understanding degradation mechanisms and improving stability in organic photovoltaics, adv. Mater. 29 (2017) 1603940.
[3] G. Yu, J. Gao, J.C. Hummelen, F. Wudl, A.J. Heeger, Polymer photovoltaic cells - enhanced efficiencies via a network of internal donor-acceptor heterojunctions, Science 270 (1995) 1789–1791.
[4] M. Jorgensen, K. Norrman, F.C. Krebs, Stability/degradation of polymer solar cells, Sol. Energ. Mat. Sol. C 92 (2008) 686–714.
[5] S. Bellani, D. Fazzi, P. Bruno, E. Giussani, E.V. Canesi, G. Lanzani, M.R. Antognazza, Reversible P3HT/oxygen charge transfer complex identification in thin films exposed to direct contact with water, J. Phys. Chem. C 118 (2014) 6291–6299.
[6] J. Schafferhans, A. Baumann, A. Wagenpfahl, C. Deibel, V. Dyakonov, Oxygen doping of P3HT:PCBM blends: influence on trap states, charge carrier mobility and solar cell performance, org. Electron. 11 (2010) 1693–1700.
[7] D.R. Kozub, K. Vakhshouri, L.M. Orme, C. Wang, A. Hexemer, E.D. Gomez, Polymer crystallization of partially miscible polythiophene/fullerene mixtures controls morphology, Macromolecules 44 (2011) 5722–5726.
[8] M. Pfannmoller, H. Flugge, G. Benner, I. Wacker, C. Sommer, M. Hanselmann, S. Schmale, H. Schmidt, F.A. Hamprecht, T. Rabe, et al., Visualizing a homogeneous blend in bulk heterojunction polymer solar cells by analytical electron microscopy, Nano Lett. 11 (2011) 3099–3107.
[9] J.D. Roehling, D. Baran, J. Sit, T. Kassar, T. Ameri, T. Unruh, C.J. Brabec, A.J. Moule, Nanoscale Morphology of PTB7 Based Organic Photovoltaics as a Function of Fullerene Size, sci. Rep. 6 (2016) 30915.
[10] J.B. Gilchrist, T.H. Basey-Fisher, S.C. Chang, F. Scheltens, D.W. mccomb, S. Heutz, Uncovering Buried Structure and Interfaces in Molecular Photovoltaics, adv. Funct. Mater. 24 (2014) 6473–6483.
[11] R.F. Egerton, P. Li, M. Malac, Radiation damage in the TEM and SEM, Micron 35 (2004) 399–409.
[12] Z.J.W.A. Leijten, A.D.A. Keizer, G. de With, H. Friedrich, Quantitative analysis of electron beam damage in organic thin films, J. Phys. Chem. C 121 (2017) 10552–10561.
[13] R.M. Glaeser, Limitations to significant information in biological electron microscopy as a result of radiation damage, J. Ultrastruct. Res. 36 (1971) 466–482.
[14] R.F. Egerton, Scattering delocalization and radiation damage in STEM-EELS, Ultramicroscopy 180 (2017) 115–124.
[15] R.F. Egerton, Vibrational-loss EELS and the avoidance of radiation damage, Ultramicroscopy 159 (2015) 95–100.
[16] R.F. Egerton, Control of radiation damage in the TEM, Ultramicroscopy 127 (2013) 100–108.
[17] B.D.A. Levin, M.J. Zachman, J.G. Werner, R. Sahore, K.X. Nguyen, Y.M. Han, B.Q. Xie, L. Ma, L.A. Archer, E.P. Giannelis, et al., Characterization of sulfur and nanostructured sulfur battery cathodes in electron microscopy without sublimation artifacts, microsc. Microanal. 23 (2017) 155–162.
[18] B. Schaffer, W. Grogger, G. Kothleitner, F. Hofer, Comparison of EFTEM and STEM EELS plasmon imaging of gold nanoparticles in a monochromated TEM, Ultramicroscopy 110 (2010) 1087–1093.
[19] M. Pfannmoller, H. Heidari, L. Nanson, O.R. Lozman, M. Chrapa, T. Offerrnans, G. Nisato, S. Bals, Quantitative tomography of organic photovoltaic blends at the nanoscale, nano Lett. 15 (2015) 6634–6642.
[20] J.B. Gilchrist, S. Heutz, D.W. mccomb, Revealing structure and electronic properties at organic interfaces using TEM, Curr. Opin. Solid St. M 21 (2017) 68–76.
[21] A.E. Goode, A.E. Porter, M.M. Klosowski, M.P. Ryan, S. Heutz, D.W. mccomb, Analytical transmission electron microscopy at organic interfaces, Curr. Opin. Solid St. M 21 (2017) 55–67.
[22] D. Chen, W. Zhao, T.P. Russell, P3HT nanopillars for organic photovoltaic devices nanoimprinted by AAO templates, Acs Nano 6 (2012) 1479–1485.
[23] H. Wu, J.L. Yang, S.L. Cao, L.L. Huang, L.H. Chen, Ordered organic nanostructures fabricated from anodic alumina oxide templates for organic bulk- heterojunction photovoltaics, Macromol. Chem. Phys. 215 (2014) 584–596.
[24] J.I. Lee, S.H. Cho, S.M. Park, J.K. Kim, J.K. Kim, J.W. Yu, Y.C. Kim, T.P. Russell, Highly aligned ultrahigh density arrays of conducting polymer nanorods using block copolymer templates, Nano Lett. 8 (2008) 2315–2320.
[25] I. Botiz, S.B. Darling, Self-Assembly of Poly(3-hexylthiophene)-block-polylactide block copolymer and subsequent incorporation of electron acceptor material, Macromolecules 42 (2009) 8211–8217.
[26] V. Vohra, M. Campoy-Quiles, M. Garriga, H. Murata, Organic solar cells based on nanoporous P3HT obtained from self-assembled P3HT:PS templates, j. Mater. Chem. 22 (2012) 20017–20025.
[27] V. Vohra, O. Notoya, T. Huang, M. Yamaguchi, H. Murata, Nanostructured poly(3-hexylthiophene-2,5-diy1) films with tunable dimensions through self-assembly with polystyrene, Polymer 55 (2014) 2213–2219.
[28] K. Gnanasekaran, R. Snel, G. de With, H. Friedrich, Quantitative nanoscopy: tackling sampling limitations in (S)TEM imaging of polymers and composites, Ultramicroscopy 160 (2016) 130–139.
[29] N. Otsu, Threshold selection method from gray-level histograms, IEEE T. Syst. Man. Cyb. 9 (1979) 62–66.
[30] S.S. van Bavel, E. Sourty, G. de With, J. Loos, Three-dimensional nanoscale organization of bulk heterojunction polymer solar cells, Nano Lett. 9 (2009) 507–513.
[31] M.J.M. Wirix, P.H.H. Bomans, M.M.R.M. Hendrix, H. Friedrich, N.A.J.M. Sommerdijk, G. de With, Visualizing order in dispersions and solid state morphology with Cryo-TEM and electron tomography: P3HT: PCBM organic solar cells, J. Mater. Chem. A 3 (2015) 5031–5040.
[32] G. Kothleitner, F. Hofer, Optimization of the signal to noise ratio in EFTEM elemental maps with regard to different ionization edge types, Micron 29 (1998) 349–357.
[33] R.F. Egerton, Electron Energy-Loss Spectroscopy in the Electron Microscope, third ed., Springer, New York, NY, 2011.
[34] U. Golla, H. Kohl, Theoretical and experimental investigations of resolution and detection limits in energy-filtering electron microscopy, Micron 28 (1997) 397–406.
[35] S. Amelinckx, D.V. Dyck, J.V. Landuyt, G.V. Tendeloo, Electron Microscopy, Principles and Fundamentals, VCH Verlagsgesellschaft mbh: Weinheim, 1997.
[36] H. Friedrich, P.M. Frederik, G. de With, N.A.J.M. Sommerdijk, Imaging of self-assembled structures: interpretation of TEM and Cryo-TEM images, Angew. Chem. Int. Edit. 49 (2010) 7850–7858.